Title

Sources of the frontocentral mismatch negativity and P3a responses in schizophrenia patients and healthy comparison subjects

Authors

Koshiyama, Daisuke
Miyakoshi, Makoto
Joshi, Yash B
et al.

Publication Date

2021-03-01

DOI

10.1016/j.ijpsycho.2021.01.005

Peer reviewed

HHS Public Access

Author manuscript

Int J Psychophysiol. Author manuscript; available in PMC 2022 March 01.

Published in final edited form as:

Int J Psychophysiol. 2021 March ; 161: 76–85. doi:10.1016/j.ijpsycho.2021.01.005.

Sources of the Frontocentral Mismatch Negativity and P3a Responses in Schizophrenia Patients and Healthy Comparison Subjects

Daisuke Koshiyama, M.D., Ph.D.[1], **Makoto Miyakoshi, Ph.D.**[2], **Yash B. Joshi, M.D., Ph.D.**[1,3], **Masaki Nakanishi, Ph.D.**[2], **Kumiko Tanaka-Koshiyama, M.D.**[1], **Joyce Sprock, B.A.**[1,3], **Gregory A. Light, Ph.D.**[1,3]

[1]Department of Psychiatry, University of California San Diego, La Jolla, CA, USA

[2]Swartz Center for Neural Computation, University of California San Diego, La Jolla, CA, USA

[3]VISN-22 Mental Illness, Research, Education and Clinical Center (MIRECC), VA San Diego Healthcare System, San Diego, CA, USA

Abstract

Background: Mismatch negativity (MMN) and P3a are event-related potential measures of early auditory information processing that are increasingly used as translational biomarkers in the development of treatments for neuropsychiatric disorders. These responses are reduced in schizophrenia patients over the frontocentral scalp electrodes and are associated with important domains of cognitive and psychosocial functioning. While MMN and P3a responses are generated by a dynamic network of cortical sources distributed across the temporal and frontal brain regions, it is not clear how these sources independently contribute to MMN and P3a at the primary frontocentral scalp electrode or to abnormalities observed in schizophrenia. This study aimed to determine the independent source contributions and characterize the magnitude of impairment in source-level MMN and P3a responses in schizophrenia patients.

Methods: A novel method was applied to back-project the contributions of 11 independent cortical source components to Fz, the primary scalp sensor that is used in clinical studies, in n=589 schizophrenia patients and n=449 healthy comparison subjects.

Corresponding Author: Makoto Miyakoshi, Ph.D., Swartz Center for Neural Computation, University of California San Diego, 9500 Gilman Drive, La Jolla, CA, USA 92093-0559, Tel.: (858) 822-7534, mmiyakoshi@ucsd.edu.

Author contributions

J. Sprock and G. Light collected the data. D. Koshiyama, M. Miyakoshi, and K. Tanaka-Koshiyama analyzed the data. M. Miyakoshi wrote the Matlab code. D. Koshiyama, M. Miyakoshi, Y Joshi, M. Nakanishi, K. Tanaka-Koshiyama, and G. Light interpreted the results. D. Koshiyama, M. Miyakoshi, and G. Light designed the study. G. Light supervised all aspects of collection, analysis, and interpretation of the data. D. Koshiyama, M. Miyakoshi, M. Nakanishi, and G. Light wrote the original manuscript. Y Joshi, K. Tanaka-Koshiyama, and J. Sprock reviewed and edited the manuscript. All authors contributed to and approved the final manuscript.

Declaration of Conflicting Interests

G. Light reported consulting for Astellas Pharma, Inc, Heptares Therapeutics, NeuroSig, Neurocrine, and Novartis.

Results: The groups showed comparable individual source contributions underlying both MMN and P3a responses at Fz. Source-level responses revealed an increasing magnitude of impairment in schizophrenia patients from the temporal to more frontal sources.

Conclusions: Schizophrenia patients have a normal architecture of source contributions that are accompanied by widespread abnormalities in source resolved mismatch and P3a responses, with more prominent deficits detected from the frontal sources. Quantification of source contributions and source-level responses accelerates clarification of the neural mechanisms underlying the networks underlying MMN reduction at Fz in schizophrenia.

Keywords

independent component analysis; mismatch negativity; P3a; schizophrenia; source-level analysis; translational biomarker

1. Introduction

Mismatch negativity (MMN) and P3a are event-related potential (ERP) measures of early auditory information processing that are markedly reduced in schizophrenia patients and robustly associated with cognitive and psychosocial functional impairment (Hochberger et al., 2019a; Javitt et al., 1995; Kim et al., 2014; Koshiyama et al., 2017, 2018a, 2018b, 2020c; Light and Braff, 2005a; Rasser et al., 2011; Salisbury et al., 2017; Thomas et al., 2017; Umbricht and Krljes, 2005; Wynn et al., 2010). MMN is a negative-going peak in the frontocentral scalp electrodes reflecting the differences in ERP responses to infrequent/physically deviant vs. frequent/standard stimuli and reflects a largely automatic (Rissling et al., 2013) and pre-attentive deviance detection process (Koshiyama et al., 2020a). MMN is usually followed by the positive P3a component that is thought to index an automatic orienting or covert shifting of attention toward infrequent novel or salient stimuli (Koshiyama et al., 2020d; Squires et al., 1975).

MMN and P3a analogs are present in a variety of model animal systems, from rodents to nonhuman primates, and are increasingly used to interrogate neural substrates in order to promote bench-to-bedside clinical translation, particularly for evaluation of novel compounds in discovery medicine (Farley et al., 2010; Featherstone et al., 2018; Fishman and Steinschneider, 2012). Due to these potential applications, MMN and P3a are promising and sensitive biomarkers of neural system engagement useful for predicting and monitoring response to central nervous system (CNS) therapeutics (Braff and Light, 2004; Hochberger et al., 2019a; Javitt et al., 2008; Lavoie et al., 2008; Light and Swerdlow, 2015; Perez et al., 2017; Swerdlow et al., 2016).

Due to convenience, MMN and P3a are sometimes reported from only a single frontocentral scalp sensor where responses tend to be largest in humans (e.g., Light et al., 2015; Thomas et al., 2017; Lainscseck et al., 2019), even when multiple channels are recorded. While MMN and P3a are sequentially elicited in the context of a passive auditory oddball paradigm (Light and Braff, 2005a) and represent dissociable responses (Koshiyama et al., 2020b; Rissling et al., 2012), they are generated by a dynamic and interactive network of cortical sources distributed across multiple temporal and frontal brain regions. Previous studies have

reported contributing sources of MMN and P3a in the auditory cortices such as the Heschl's gyrus and the superior temporal gyrus, the frontal cortex (i.e., the orbitofrontal and inferior frontal cortices), and the anterior and middle cingulate gyri (Gaebler et al., 2015; Mathiak et al., 2002; Miyanishi et al., 2013; Molholm et al., 2005; Oknina et al., 2005; Opitz et al., 2002; Rissling et al., 2014; Schall et al., 2003; Takahashi et al., 2013; Yamasue et al., 2004; Youn et al., 2003). Furthermore, a macro circuit involving multiple regions such as the temporal and frontal gyri in a predictive coding framework was suggested (Corlett et al., 2011; Garrido et al., 2008; MacLean and Ward, 2014; Phillips et al., 2015; Randeniya et al., 2018; Sterzer et al., 2018; Tada et al., 2019). In this framework, the network of the auditory cortex, the superior temporal cortex, and the inferior frontal cortex identified via dynamic causal modeling was impaired in schizophrenia patients (Dima et al., 2012). Whereas our recent connectivity-based analyses characterized the dynamic flow of information among multiple highly interactive temporal and frontal brain sources (Koshiyama et al., 2020b), no study has yet identified the independent source contributions to MMN and P3a measured at the frontocentral electrode (Fz) or quantified source-level mismatch and P3a responses in schizophrenia patients or healthy comparison subjects.

This study aimed to 1) identify and compare the independent source contributions to the frontocentral MMN and P3a amplitude, and 2) characterize the magnitude of impairment of source-resolved MMN and P3a responses in schizophrenia patients relative to healthy comparison subjects using source-level electroencephalogram (EEG) data-driven approach. We hypothesized that schizophrenia patients would have an abnormal mixture of source contributions from the temporal and frontal regions (i.e., the superior temporal cortex, the orbitofrontal cortex, and the anterior and middle cingulate cortices) to MMN and P3a responses at Fz and that impairments in schizophrenia patients would be more prominent among the frontal sources.

2. Methods and materials

2.1. Subjects

Participants consisted of an archival cohort of 589 schizophrenia patients and 449 healthy comparison subjects. The mean age of patients (413 male/176 female) was 45.6 (standard deviation (SD) 9.9; range 19–72) years old. The mean age of healthy comparison subjects (217 male/232 female) was 43.6 (SD 12.8; range 18–85) years old. Of the 589 participants, 530 were stabilized on antipsychotic medications. Study inclusion/exclusion criteria and detailed demographic characteristics are described in Koshiyama et al. (2020b) and Supplementary Methods. Written informed consent was obtained from each subject. The Institutional Review Board of University of California San Diego approved all experimental procedures (071128, 071831, 170147).

2.2. Auditory Oddball Paradigm

MMN and P3a were evoked via a passive auditory oddball paradigm following our established procedures (Light and Braff, 2005a, b). Subjects were presented with binaural tones (1-kHz, 85-dB, with 1-ms rise/fall, stimulus onset asynchrony 500 ms) via inserted earphones (Aearo Company Auditory Systems, Indianapolis, IN; Model 3A). During the

approximately 20-min session, participants watched a silent cartoon video. Participants were instructed to attend to the video as they might be asked to answer questions about it at the end of the session. Standard (p = 0.90, 50-ms duration) and Deviant (p = 0.10, 100-ms duration) tones were presented in a pseudorandom order with a minimum of 6 Standard stimuli presented between each Deviant stimulus.

2.3. Electroencephalography recording and preprocessing

EEG data were continuously digitized at a rate of 500 Hz (nose reference, forehead ground) using a 40-channel Neuroscan system (Neuroscan Laboratories, El Paso, Texas). The electrode montage was based on standard positions in the International 10–5 electrode system (Oostenveld and Praamstra, 2001) fitted to the Montreal Neurological Institute (MNI) template head used in EEGLAB, including AFp10 and AFp9 as horizontal electrooculogram (EOG) channels, Inferior and superior EOGs above and below the left eye as vertical EOG channels, Fp1, Fp2, F7, F8, Fz, F3, F4, FC1, FC2, FC5, FC6, C3, Cz, C4, CP1, CP2, CP5, CP6, P7, P3, Pz, P4, P8, T7, T8, TP9, TP10, FT9, FT10, PO9, PO10, O1, O2, and Iz. Electrode-to-skin impedance mediated by conductive gel was brought below 4 kΩ. The system acquisition bandpass was 0.5–100 Hz. Offline, EEG data were imported to EEGLAB 14.1.2 (Delorme and Makeig, 2004) running under Matlab 2017b (The MathWorks, Natick, MA). The data were high-pass filtered (finite impulse response (FIR), Hamming window, cutoff frequency 0.5 Hz, transition bandwidth 0.5). EEGLAB plugin *clean_rawdata()* including Artifact Subspace Reconstruction (ASR) was applied to reduce high-amplitude artifacts (Blum et al., 2019; Chang et al., 2018, 2020; Gabard-Durnam et al., 2018; Kothe and Makeig, 2013; Mullen et al., 2015). The parameters used were: flat line removal, 10 s; electrode correlation, 0.7; ASR, 20; window rejection, 0.5. The mean channel rejection rate was 4.5 % (SD 3.0, range 0–15.8). The mean data rejection rate was 3.1% (SD 3.9, range 0–28.7). The rejected channels were interpolated using EEGLAB's spline interpolation function. Data were re-referenced to average. Adaptive mixture independent component analysis (ICA; Bell and Sejnowski, 1995; Delorme et al., 2012) was applied to the preprocessed scalp recording data to obtain temporally maximally independent components. For the scalp topography of each independent component derived, the equivalent current dipole was estimated using Fieldtrip functions (Oostenveld et al., 2011). For scalp topographies more suitable for symmetrical bilateral dipoles, two symmetrical dipoles were estimated (Piazza et al., 2016). To select brain independent components (ICs) among all types of ICs, EEGLAB plugin *ICLabel()* was used (Pion-Tonachini et al., 2019). The inclusion criteria were 1) 'brain' label probability > 0.8 and 2) residual variance i.e., var((actual scalp topography) – (theoretical scalp projection from the fitted dipole))/ var(actual scalp topography) < 0.10. A total of 11096 ICs was preselected as representative brain ICs (mean 10.7 ICs per individual, SD 4.1, range 1–37). The data was epoched from −100 to 500 ms relative to stimulus onset. The mean number of standard stimuli was 2462 (SD 484, range 1546–5398), and that for the deviant condition was 266 (SD 52, range 156–538).

For group-level analysis, k-means clustering was applied to the matrix of 11096 × 3 dimensions that is number of ICs times x, y, z coordinates of the estimated location of equivalent current dipoles. When two laterally symmetrical dipoles were estimated, one of

the sides that showed a larger dipole moment was selected. To determine optimal number of clusters, the silhouette algorithm was used and resulted in the identification of 11 independent source-clusters (Rousseeuw, 1987).

2.4. Calculating MMN and P3a at Fz and each source cluster

ERP amplitudes were quantified for the combination of each cluster (plus the scalp electrode at Fz referenced to average potential), group, and condition. The signal recorded at Fz was reconstructed by back-projecting the pre-selected brain ICs; contributions by non-brain components were excluded. The obtained ERPs of the standard tone condition were subtracted from those of the deviant tone condition to obtain the difference amplitudes (i.e., MMN and P3a amplitudes). For each IC, the mean amplitude from 135 ms to 205 ms was averaged to obtain MMN amplitude, and that from 250 ms to 300 ms was averaged to obtain P3a amplitude. The difference amplitudes were averaged across all ICs that belong to the same combination of cluster/electrode and group to obtain their representative values.

2.5. Quantifying independent source contribution to MMN and P3a at Fz

Most approaches to identifying sources of ERP signals rely upon the full scalp topography of EEG responses and apply the inverse solution. These frameworks and their resulting source-level responses, however, yield “super-additive” components that account for more than 100% of the variance due to some overlap. Using the framework of ICA, we applied a novel method that benefits from the wealth of information contained in the whole EEG data including the full scalp topography, and characterized the independent source contributions to the commonly studied frontocentral electrode Fz. In this framework, no super-additivity is observed; potentials at scalp electrodes are expressed as a sum of contributions from all independent component (IC) sources that survived the abovementioned pre-selection as

$$\boldsymbol{WX} = \boldsymbol{Y}, \tag{1}$$

where $\boldsymbol{X} = [x_1(t), x_2(t), \cdots, x_I(t)]^T \in \mathbb{R}^{I \times T}$ represents scalp-electrode signals, which is in the current case ERP difference waves from deviance minus standard by the definition of MMN and P3a, $\boldsymbol{W} = \left(w_{j,i}\right)_{1 \le i \le I}^{1 \le j \le J} \in \mathbb{R}^{J \times I}$ represents an unmixing matrix estimated by ICA (in EEGLAB, EEG.icaweights*EEG.icasphere; EEG.icaweights refers to the mixing matrix obtained by ICA (dimension: ICs × data rank); EEG.icasphere refers to the sphering matrix that is applied to multivariate scalp-electrode data as a preprocessing for ICA (dimension: electrodes × data rank)), and $\boldsymbol{Y} = [y_1(t), y_2(t), \cdots, y_J(t)]^T \in \mathbb{R}^{J \times T}$ represents ICA-decomposed source activations (in EEGLAB, EEG.icaact; EEG.icaact refers to the IC time activation (dimension: ICs × data points)). Here, I is the number of electrodes, J is the number of ICs, and T is the number of sampling points. In this study, I was 40, and T was set to 151 so as to cover from −100 ms to 500 ms at a sampling rate of 250 Hz relative to the onset of each stimulus. The theoretical maximum number of ICs J is equal to or less than the number of the scalp electrodes (i.e., $J \le I$) and may differ from subject to subject because of the artifact IC rejection performed using *ICLabel()*. The scalp activities may be reconstructed by back-projecting all the IC source activities as

$$\widetilde{\boldsymbol{X}} = \boldsymbol{W}^{+}\boldsymbol{Y}, \tag{2}$$

where $\boldsymbol{W}^{+} = \left(w_{i,j}^{+}\right)_{1 \le j \le J}^{1 \le i \le I} \in \mathbb{R}^{I \times J}$ is the pseudoinverse of $\boldsymbol{W}$.

The time window of interest in the current study was divided into two windows for MMN ($60 \le t \le 77$) and P3a ($89 < t \le 101$), which correspond to 135–205 ms and 250–300 ms relative to the onset of each stimulus, respectively.

We are interested in obtaining the ratio of root-mean-square (RMS) values of the scalp ERP reconstructed from each IC activation across J back-projected IC-ERPs at one of the scalp electrodes (i.e., Fz) during the time-window of MMN and P3a. The j-th IC source ERP back-projected to the i-th electrode is written as

$$\tilde{x}_{i,j}(t) = w_{i,j}^{+} y_j(t)\,. \tag{3}$$

The RMS value of $\tilde{x}_{i,j}(t)$ for the time window of interest, written as $\mathrm{RMS}_{i,j}$, is calculated as

$$\mathrm{RMS}_{i,j} = \sqrt{\frac{1}{t_2 - t_1}\sum_{t=t_1}^{t_2}\left(\tilde{x}_{i,j}(t)\right)^2}, \tag{4}$$

where the two time windows of interests were $[t_1\ t_2] = [60\ 77]$ for MMN and $[t_1\ t_2] = [89\ 101]$ for P3a. Within-subject normalized RMS-contribution of the j-th IC to i-th electrode $\overline{\mathrm{RMS}}_{i,j}$ was calculated as

$$\overline{\mathrm{RMS}}_{i,j} = \frac{\mathrm{RMS}_{i,j}}{\sum_{h=1}^{J}\mathrm{RMS}_{i,h}}\,. \tag{5}$$

Thus, each IC source's contribution to one of the scalp electrodes is represented as a percentage and $\sum_{j=1}^{J}\overline{\mathrm{RMS}}_{i,j} = 1$.

The within-subject percentage-normalized RMS values were calculated for all ICs, then gathered at the group-level analysis. The collected RMS ratios $\overline{\mathrm{RMS}}$ defined by eq.(5) from all the subjects were sub-grouped into 11 clusters along with the ICs. Let C_m be the label of m-th clusters, $\bar{J}_m$ be the number of ICs in m-th cluster, and M be the number of clusters (i.e., $M = 11$ and $\sum_{m=1}^{M}\bar{J}_m = 11096$ in this study), cluster-mean of $\overline{\mathrm{RMS}}$ in m-th cluster $\widetilde{\overline{\mathrm{RMS}}}_m$ was calculated as

$$\widetilde{\overline{\mathrm{RMS}}}_m = \frac{1}{\bar{J}_m}\sum_{\overline{\mathrm{RMS}} \subset C_m}\overline{\mathrm{RMS}}\,. \tag{6}$$

$\widetilde{\overline{\mathrm{RMS}}}_m$ was further normalized across clusters into percentage as

$$\widehat{\mathrm{RMS}}_m = \frac{\widetilde{\mathrm{RMS}}_m}{\sum_{l=1}^{M} \widetilde{\mathrm{RMS}}_l}. \tag{7}$$

Thus, each IC cluster's contribution to i-th electrode was expressed as a re-normalized percentage and $\sum_{m=1}^{M} \widehat{\mathrm{RMS}}_m = 1$. This $\widehat{\mathrm{RMS}}_m$ was calculated for each group separately for statistical testing.

Finally, the cluster-wise contribution to a single electrode was calculated. Let $\boldsymbol{x}_i^{(n)} \in \mathbb{R}^T$ be the n-th subject's scalp-recording at i-th electrode and $\tilde{\boldsymbol{x}}_{i,j}^{(n)} \in \mathbb{R}^T$ be the n-th subject's k-th IC source ERP back-projected to the i-th electrode, the relation between them is such that from ICA's property,

$$\sum_{n=1}^{N} \sum_{j=1}^{J} \tilde{\boldsymbol{x}}_{i,j}^{(n)} = \sum_{n=1}^{N} \boldsymbol{x}_i^{(n)}, \tag{8}$$

where N represents the number of subjects for each group (i.e., 449 and 589 for healthy comparison subjects and patients, respectively). For each of m-th cluster C_m, there were $\bar{J}_m$ ICs and $\bar{J}_m$ back-projected IC-source ERPs $\tilde{\boldsymbol{x}}_{i,j}^{(n)}$ from N subjects. This cluster's average ERP projection to a single electrode $\boldsymbol{Z}_{i,m} \in \mathbb{R}^T$ is calculated as

$$\boldsymbol{Z}_{i,m} = \frac{1}{\bar{J}_m} \sum \tilde{\boldsymbol{x}}_{i,j}^{(n)} \subset C_m \tilde{\boldsymbol{x}}_{i,j}^{(n)}. \tag{9}$$

This $\boldsymbol{Z}_{i,m}$ was calculated for each IC cluster and each group separately. It represents a single IC cluster's mean root-mean-squared ERP contribution ratio to a single electrode. The relation between $\boldsymbol{Z}_{i,m}$ and signal-channel ERPs is such that

$$\sum_{m=1}^{M} \boldsymbol{Z}_{i,m} \cong \frac{1}{N} \sum_{n=1}^{N} \boldsymbol{x}_i^{(n)}. \tag{10}$$

The left-hand side and the right-hand side do not match because averaging on $\tilde{\boldsymbol{x}}_{i,j}^{(n)} \subset C_m$ has an effect of additional weighting from the group-level analysis so that it violates the within-subject linear-sum assumption between IC sources and scalp electrodes. In this study, $i = 9$ to refer to Fz. Subsequently, statistical tests were performed between the groups for each of the 11 clusters.

2.6. Statistical analysis

Two-sample t-tests were used to compare groups (healthy comparison subjects and schizophrenia patients) on measures of MMN and P3a at Fz, MMN and P3a in the estimated source components of scalp Fz, and the root-mean-squared ERP contribution ratio (%) to the electrode of the Fz in the source components. Cohen's d was used to assess effect sizes. Statistical significance was set at $p < 0.05$ adjusted to false discovery rate with 2 responses

for MMN and P3a amplitude (μV) at Fz, and set at $p < 0.05$ adjusted to false discovery rate with 2 responses × 11 source locations for MMN and P3a amplitude (μV) at source locations as well as for the contribution rate (%) of MMN and P3a to those at Fz.

3. Results

3.1. MMN and P3a at scalp Fz

ERP elicited by standard stimuli and ERP by deviant stimuli at Fz in healthy comparison subjects and schizophrenia patients are shown in Figure 1. Both MMN ($d = -0.55$, $p = 1.1 \times 10^{-18}$) and P3a ($d = 0.61$, $p = 2.0 \times 10^{-22}$) amplitude at Fz were significantly reduced in schizophrenia patients relative to healthy comparison subjects (Table 1, Figure 2). MMN and P3a amplitudes reflect back-projected surface potential estimates at Fz using an average reference.

3.2. MMN and P3a at source components of scalp Fz

The coordinates of the 11 contributing IC clusters are shown in Supplementary Table 1. ERP elicited by standard stimuli and ERP by deviant stimuli in each source component in healthy comparison subjects and schizophrenia patients are reported in Supplementary Figure 1 and Supplementary Figure 2. Source component amplitudes of MMN at scalp Fz were significantly reduced in the right inferior temporal gyrus ($d = -0.21$, $p = 0.016$), left middle temporal gyrus ($d = -0.30$, $p = 1.7 \times 10^{-5}$), left superior temporal gyrus ($d = -0.26$, $p = 0.001$), right precentral gyrus ($d = -0.15$, $p = 0.012$), middle cingulate gyrus ($d = -0.35$, $p = 4.8 \times 10^{-7}$), orbitofrontal cortex ($d = -0.36$, $p = 3.0 \times 10^{-9}$) and anterior cingulate gyrus ($d = -0.52$, $p = 2.5 \times 10^{-12}$) in schizophrenia patients relative to healthy comparison subjects (Table 1, Figure 2). Source component amplitudes of P3a at scalp Fz were additionally reduced in the right primary visual cortex ($d = 0.46$, $p = 5.4 \times 10^{-13}$) and the left middle temporal gyrus ($d = 0.24$, $p = 4.6 \times 10^{-4}$), posterior cingulate gyrus ($d = 0.16$, $p = 0.003$), middle cingulate gyrus ($d = 0.31$, $p = 6.1 \times 10^{-6}$), orbitofrontal cortex ($d = 0.24$, $p = 8.8 \times 10^{-5}$) and anterior cingulate gyrus ($d = 0.47$, $p = 2.1 \times 10^{-10}$) in schizophrenia patients relative to healthy comparison subjects. (Table 1, Figure 2). A sum of these 11 MMN and P3a source components is equivalent to MMN and P3a at Fz in each group.

3.3. Contribution weight of source components to scalp Fz

Contribution rates of source components to MMN and P3a at scalp Fz are shown in Table 2 and Figure 3. While the contribution weight of MMN source components was not significantly different between groups, schizophrenia patients showed a slightly reduced contribution weight of the middle cingulate gyrus to P3a response (9.3 % vs. 11.9%; $p = 5.0 \times 10^{-4}$).

4. Discussion

This study applied a novel method of independent source deconstruction to the widely studied MMN and P3a responses in schizophrenia patients and healthy subjects. While we anticipated that patients would show abnormal source contribution weight to the frontocentral scalp responses, the groups showed nearly identical contribution weight of

each source; only the middle cingulate cortex contribution ratio to the P3a response was slightly reduced in schizophrenia patients relative to healthy comparison subjects (i.e., 9.3 % vs. 11.9 %). While this data did not generally support our hypothesis of an abnormal mix of the source contribution weight to scalp MMN and P3a impairments in schizophrenia, they nevertheless add to a more comprehensive understanding of signal processing in health and illness. It is interesting to note that the middle cingulate cortex demonstrated slightly reduced contribution weight to P3a in schizophrenia patients relative to healthy comparison subjects. The middle cingulate cortex is known to be involved in social cognition in healthy non-psychiatric adults (Blakemore, 2008); we speculate that the middle cingulate contributions in the processing of sensory information may be associated with social cognition impairment in schizophrenia patients.

Whereas neural responses to auditory sensory stimuli are generated by the temporal sources, primary contribution weight to MMN and P3a at Fz calculated from duration deviant-minus-standard difference waves was located in the orbitofrontal cortex and the anterior cingulate gyrus in both groups, consistent with other source-imaging methods (e.g., eLORETA; Takahashi et al., 2013). The back-projection quantification of source-level ERP amplitudes computed via this method revealed that ERP amplitude reduction in schizophrenia is distributed over across multiple brain regions, with more marked impairments evident from the frontal regions. Specifically, source-resolved MMN amplitude deficits were detected in the temporofrontal cortices and the precentral gyrus; P3a was significantly reduced in the temporofrontal cortices as well as near the primary visual cortex and posterior cingulate gyrus in schizophrenia.

In the perspective of the predictive coding framework, the temporofrontal regions are presumed to play an important role (Garrido et al., 2008; Phillips et al., 2015). Koshiyama et al. (2020a) showed selective impairments in deviance detection but no impairment in adaptation to repeated tones in schizophrenia patients. A prior electrocorticographic study reported a source location of adaptation at the superior temporal cortex and that of deviance detection both at the temporal and prefrontal cortices (Ishishita et al., 2019). Thus, adaptation to repeated tones may be processed at the temporal region, with the frontal regions involved in prediction errors. Future source-level studies are needed to deconstruct sensory adaptation, deviance detection, and prediction error processes.

The methodologic approach for quantifying source contributions as well as source-level responses to EEG recordings presented in this report represents a promising advance for precise biomarker development. In order to quantify the contribution of ICs at the individual subject level, RMS values within the time windows of interest were calculated. The purpose of this approach was to obtain non-negative measures that have clear physical meaning; amplitude in alternative current (AC) is converted to that of direct current (DC). Attempts to quantify contributions of IC sources to scalp electrodes have largely been conducted by calculating *percent variance accounted for* (PVAF) across scalp electrodes (Lee et al., 2015; Rissling et al., 2014). However, the calculation of PVAF uses variance across all scalp electrodes for each time frame, which is not applicable to single scalp electrode analysis. Moreover, averaging the variance across time tends to make this metric's behavior unpredictable; for example, PVAF could yield negative values, which does not make

intuitive sense (Koshiyama et al., 2020b). Therefore, PVAF has a limitation—decomposed ERPs are signed signals (in μV); hence they cancel each other in the process of mixing. This makes the metric of PVAF super-additive due to triangular inequity (i.e., $a^2+b^2 > (a+b)^2$), and the underlying signal cancellation makes it difficult to interpret the results (Lee et al., 2015). Compared with this approach, the calculating RMS has an advantage over the method, thanks to non-negativity. The simple additive nature of this metric makes it suitable to be normalized into a percentage to emphasize the relative ratio of contributions in contrast with other contributing sources. The clear physical meaning of RMS also provides an intuitive understanding of the meaning of the metric.

4.1. Limitations

Findings from this study should be considered in the context of several limitations. First, this was a cross-sectional cohort study of a heterogeneous sample of patients in whom medications were not experimentally controlled. Second, patients with schizophrenia were relatively chronic in this study. As such, results may not generalize to individuals with early psychosis or at risk for psychosis. Even in chronic patients, there was no qualitative difference in the neuronal generator pattern between patients and healthy subjects; they may have similar generator patterns relative to healthy subjects. Third, we employed only 40 channels for source-level analyses. As discussed previously (Hochberger et al., 2019b; Hochberger et al., 2020; Lainscsek et al., 2019), 64 channels are preferred for the application of modem signal processing techniques in order to remove artifacts and thereby improve the signal to noise ratios for both scalp- and source-level responses, even if only a single scalp channel is of primary interest (Thomas et al., 2017). The limited EEG montage has the potential to be a reason for similar source configurations between groups. Moreover, the use of higher density arrays will allow for a more precise decomposition of sources as well as source-level responses. Since the present results represent a back projection of Fz rather than a complete decomposition of scalp topography, findings do not readily allow for a direct comparison with other methods (e.g., eLORETA). Nonetheless, the primary independent sources identified here have also been consistently observed via a variety of techniques. Fourth, source analyses were conducted across a full 1–500 ms auditory deviance response complex; the results of estimated source locations may contain contributions from MMN, P3a, reorienting negativity (RON), and perhaps N100. During the period of 500 ms when the ERP component appears, it is probable that some dominant current sources appear, disappear, and move temporally. Therefore, we could not discuss the difference of source locations between MMN and P3a in this study. Fifth, our findings using the duration deviant paradigm may not fully generalize to MMN elicited by other types of deviants (i.e., frequency deviants). Previous studies reported that MMN elicited by duration deviants (but not frequency deviants) could be a biological predictor of future psychosis onset in individuals with clinical high-risk, which may be used for early detection and intervention of psychosis (Bodatsch et al., 2015; Tateno et al., 2020). Further investigation focusing on the difference between deviant types may provide fruitful findings. Sixth, although visual processing areas only provided 5–6 % contribution weight to the frontocentral scalp response, this contribution was not expected in the context of a passive auditory oddball task. In a broader context, the occipital region with the primary visual cortex (V1) was known as the major area of abnormalities in studies of visual processing in schizophrenia

(Butler et al., 2001; Martinez et al., 2008). Morita et al. (2019) demonstrated the association between eye movement impairments and the reduced gray matter cortical thickness in schizophrenia patients in the lateral occipital cortex. Although speculative, patients with schizophrenia may show simultaneous impairments of various perception-related brain regions (i.e., auditory and visual processing), which may ultimately contribute to aberrant salience (i.e., hallucinations and delusions). Lastly, the magnitude of MMN and P3a impairments measured at Fz (absolute values of $d = 0.55–0.61$) was smaller than that shown in previous studies ($\sim d = 1.0$; Umbricht and Krljes, 2005). It is possible that the more rigorous data preprocessing approach of pruning potential artifactual independent components at the level of individual subjects and groups necessary for the source analysis may have attenuated Fz effect sizes.

4.2. Conclusion

This study showed independent source deconstruction of MMN and P3a amplitude in schizophrenia patients and healthy comparison subjects. Despite marked reductions in the frontocentral scalp and source-level responses, patients with schizophrenia provide comparable source contributions to MMN and P3a responses at the primary Fz electrode. The largest contributors to responses at Fz are located in the orbitofrontal and the anterior cingulate gyrus in both groups. Results fill in the knowledge gap between previous MMN studies measured at Fz and those from source-level studies of MMN and accelerate clarification of the neural mechanisms underlying the networks underlying MMN reduction at Fz in schizophrenia patients.

Supplementary Material

Refer to Web version on PubMed Central for supplementary material.

Acknowledgments

Funding

This study was supported by JSPS Overseas Research Fellowships (D. K), the Sidney R. Baer, Jr. Foundation, the Brain and Behavior Research Foundation, grants from NIMH (MH79777, MH042228) and the VISN-22 Mental Illness, Research, Education, and Clinical Center (G. L). Swartz Center for Computational Neuroscience is supported by a generous gift of the Swartz Foundation.

References

Bell AJ, Sejnowski TJ, 1995. An information-maximization approach to blind separation and blind deconvolution. Neural Comput 7, 1129–1159. [PubMed: 7584893]

Blakemore SJ, 2008. The social brain in adolescence. Nat Rev Neurosci 9, 267–277. [PubMed: 18354399]

Blum S, Jacobsen NSJ, Bleichner MG, Debener S, 2019. A Riemannian Modification of Artifact Subspace Reconstruction for EEG Artifact Handling. Front Hum Neurosci 13, 141. [PubMed: 31105543]

Bodatsch M, Brockhaus-Dumke A, Klosterkotter J, Ruhrmann S, 2015. Forecasting psychosis by event-related potentials-systematic review and specific meta-analysis. Biol Psychiatry 77, 951–958. [PubMed: 25636178]

Braff DL, Light GA, 2004. Preattentional and attentional cognitive deficits as targets for treating schizophrenia. Psychopharmacology (Berl) 174, 75–85. [PubMed: 15118804]

Butler PD, Schechter I, Zemon V, Schwartz SG, Greenstein VC, Gordon J, Schroeder CE, Javitt DC, 2001. Dysfunction of early-stage visual processing in schizophrenia. Am J Psychiatry 158, 1126–1133. [PubMed: 11431235]

Chang CY, Hsu SH, Pion-Tonachini L, Jung TP, 2018. Evaluation of Artifact Subspace Reconstruction for Automatic EEG Artifact Removal. Conf Proc IEEE Eng Med Biol Soc 2018, 1242–1245.

Chang CY, Hsu SH, Pion-Tonachini L, Jung TP, 2020. Evaluation of Artifact Subspace Reconstruction for Automatic Artifact Components Removal in Multi-channel EEG Recordings. IEEE Trans Biomed Eng 67, 1114–1121. [PubMed: 31329105]

Corlett PR, Honey GD, Krystal JH, Fletcher PC, 2011. Glutamatergic model psychoses: prediction error, learning, and inference. Neuropsychopharmacology 36, 294–315. [PubMed: 20861831]

Delorme A, Makeig S, 2004. EEGLAB: an open source toolbox for analysis of single-trial EEG dynamics including independent component analysis. J Neurosci Methods 134, 9–21. [PubMed: 15102499]

Delorme A, Palmer J, Onton J, Oostenveld R, Makeig S, 2012. Independent EEG sources are dipolar. PLoS One 7, e30135. [PubMed: 22355308]

Dima D, Frangou S, Burge L, Braeutigam S, James AC, 2012. Abnormal intrinsic and extrinsic connectivity within the magnetic mismatch negativity brain network in schizophrenia: a preliminary study. Schizophr Res 135, 23–27. [PubMed: 22264684]

Farley BJ, Quirk MC, Doherty JJ, Christian EP, 2010. Stimulus-specific adaptation in auditory cortex is an NMDA-independent process distinct from the sensory novelty encoded by the mismatch negativity. J Neurosci 30, 16475–16484. [PubMed: 21147987]

Featherstone RE, Melnychenko O, Siegel SJ, 2018. Mismatch negativity in preclinical models of schizophrenia. Schizophr Res 191, 35–42. [PubMed: 28768598]

Fishman YI, Steinschneider M, 2012. Searching for the mismatch negativity in primary auditory cortex of the awake monkey: deviance detection or stimulus specific adaptation? J Neurosci 32, 15747–15758. [PubMed: 23136414]

Gabard-Durnam LJ, Mendez Leal AS, Wilkinson CL, Levin AR, 2018. The Harvard Automated Processing Pipeline for Electroencephalography (HAPPE): Standardized Processing Software for Developmental and High-Artifact Data. Front Neurosci 12, 97. [PubMed: 29535597]

Gaebler AJ, Mathiak K, Koten JW Jr., Konig AA, Koush Y, Weyer D, Depner C , Matentzoglu S, Edgar JC, Willmes K, Zvyagintsev M, 2015. Auditory mismatch impairments are characterized by core neural dysfunctions in schizophrenia. Brain 138, 1410–1423. [PubMed: 25743635]

Garrido MI, Friston KJ, Kiebel SJ, Stephan KE, Baldeweg T, Kilner JM, 2008. The functional anatomy of the MMN: a DCM study of the roving paradigm. Neuroimage 42, 936–944. [PubMed: 18602841]

Hochberger WC, Joshi YB, Thomas ML, Zhang W, Bismark AW, Treichler EBH, Tarasenko M, Nungaray J, Sprock J, Cardoso L, Swerdlow N, Light GA, 2019a. Neurophysiologic measures of target engagement predict response to auditory-based cognitive training in treatment refractory schizophrenia. Neuropsychopharmacology 44, 606–612. [PubMed: 30377381]

Hochberger WC, Joshi YB, Zhang W, Thomas ML, Braff DL, Swerdlow NR, Light GA, 2019b. Decomposing the constituent oscillatory dynamics underlying mismatch negativity generation in schizophrenia: Distinct relationships to clinical and cognitive functioning. Int J Psychophysiol 145, 23–29. [PubMed: 30586570]

Hochberger WC, Thomas ML, Joshi YB, Swerdlow NR, Braff DL, Gur RE, Gur RC, Light GA, 2020. Deviation from expected cognitive ability is a core cognitive feature of schizophrenia related to neurophysiologic, clinical and psychosocial functioning. Schizophr Res 215, 300–307. [PubMed: 31744751]

Ishishita Y, Kunii N, Shimada S, Ibayashi K, Tada M, Kirihara K, Kawai K, Uka T, Kasai K, Saito N, 2019. Deviance detection is the dominant component of auditory contextual processing in the lateral superior temporal gyrus: A human ECoG study. Hum Brain Mapp 40, 1184–1194. [PubMed: 30353997]

Javitt DC, Doneshka P, Grochowski S, Ritter W, 1995. Impaired mismatch negativity generation reflects widespread dysfunction of working memory in schizophrenia. Arch Gen Psychiatry 52, 550–558. [PubMed: 7598631]

Javitt DC, Spencer KM, Thaker GK, Winterer G, Hajos M, 2008. Neurophysiological biomarkers for drug development in schizophrenia. Nat Rev Drug Discov 7, 68–83. [PubMed: 18064038]

Kim M, Kim SN, Lee S, Byun MS, Shin KS, Park HY, Jang JH, Kwon JS, 2014. Impaired mismatch negativity is associated with current functional status rather than genetic vulnerability to schizophrenia. Psychiatry Res 222, 100–106. [PubMed: 24650450]

Koshiyama D, Kirihara K, Tada M, Nagai T, Fujioka M, Ichikawa E, Ohta K, Tani M, Tsuchiya M, Kanehara A, Morita K, Sawada K, Matsuoka J, Satomura Y, Koike S, Suga M, Araki T, Kasai K, 2018a. Electrophysiological evidence for abnormal glutamate-GABA association following psychosis onset. Transl Psychiatry 8, 211. [PubMed: 30297786]

Koshiyama D, Kirihara K, Tada M, Nagai T, Fujioka M, Koike S, Suga M, Araki T, Kasai K, 2018b. Association between mismatch negativity and global functioning is specific to duration deviance in early stages of psychosis. Schizophr Res 195, 378–384. [PubMed: 28986006]

Koshiyama D, Kirihara K, Tada M, Nagai T, Fujioka M, Usui K, Araki T, Kasai K, 2020a. Reduced Auditory Mismatch Negativity Reflects Impaired Deviance Detection in Schizophrenia. Schizophr Bull 46, 937–946. [PubMed: 32072183]

Koshiyama D, Kirihara K, Tada M, Nagai T, Koike S, Suga M, Araki T, Kasai K, 2017. Duration and frequency mismatch negativity shows no progressive reduction in early stages of psychosis. Schizophr Res 190, 32–38. [PubMed: 28314681]

Koshiyama D, Miyakoshi M, Joshi YB, Molina JL, Tanaka-Koshiyama K, Sprock J, Braff DL, Swerdlow NR, Light GA, 2020b. Abnormal Effective Connectivity Underlying Auditory Mismatch Negativity Impairments in Schizophrenia. Biol Psychiatry Cogn Neurosci Neuroimaging 5, 1028–1039. [PubMed: 32830097]

Koshiyama D, Miyakoshi M, Thomas ML, Joshi YB, Molina JL, Tanaka-Koshiyama K, Sprock J, Braff DL, Swerdlow NR, Light GA, 2020c. Unique contributions of sensory discrimination and gamma synchronization deficits to cognitive, clinical, and psychosocial functional impairments in schizophrenia. Schizophr Res. (in press).

Koshiyama D, Thomas ML, Miyakoshi M, Joshi YB, Molina JL, Tanaka-Koshiyama K, Sprock J, Braff DL, Swerdlow NR, Light GA, 2020d. Hierarchical Pathways from Sensory Processing to Cognitive, Clinical, and Functional Impairments in Schizophrenia. Schizophr Bull. (in press).

Kothe CA, Makeig S, 2013. BCILAB: a platform for brain-computer interface development. J Neural Eng 10, 056014. [PubMed: 23985960]

Lainscsek C, Sampson AL, Kim R, Thomas ML, Man K, Lainscsek X, Swerdlow NR, Braff DL, Sejnowski TJ, Light GA, 2019. Nonlinear dynamics underlying sensory processing dysfunction in schizophrenia. Proc Natl Acad Sci U S A 116, 3847–3852. [PubMed: 30808768]

Lavoie S, Murray MM, Deppen P, Knyazeva MG, Berk M, Boulat O, Bovet P, Bush AI, Conus P, Copolov D, Fornari E, Meuli R, Solida A, Vianin P, Cuenod M, Buclin T, Do KQ, 2008. Glutathione precursor, N-acetyl-cysteine, improves mismatch negativity in schizophrenia patients. Neuropsychopharmacology 33, 2187–2199. [PubMed: 18004285]

Lee C, Miyakoshi M, Delorme A, Cauwenberghs G, Makeig S, 2015. Non-parametric group-level statistics for source-resolved ERP analysis. Conf Proc IEEE Eng Med Biol Soc 2015, 7450–7453.

Light GA, Braff DL, 2005a. Mismatch negativity deficits are associated with poor functioning in schizophrenia patients. Arch Gen Psychiatry 62, 127–136. [PubMed: 15699289]

Light GA, Braff DL, 2005b. Stability of mismatch negativity deficits and their relationship to functional impairments in chronic schizophrenia. Am J Psychiatry 162, 1741–1743. [PubMed: 16135637]

Light GA, Swerdlow NR, 2015. Future clinical uses of neurophysiological biomarkers to predict and monitor treatment response for schizophrenia. Ann N Y Acad Sci 1344, 105–119. [PubMed: 25752648]

Light GA, Swerdlow NR, Thomas ML, Calkins ME, Green MF, Greenwood TA, Gur RE, Gur RC, Lazzeroni LC, Nuechterlein KH, Pela M, Radant AD, Seidman LJ, Sharp RF, Siever LJ, Silverman JM, Sprock J, Stone WS, Sugar CA, Tsuang DW, Tsuang MT, Braff DL, Turetsky BI, 2015. Validation of mismatch negativity and P3a for use in multi-site studies of schizophrenia: characterization of demographic, clinical, cognitive, and functional correlates in COGS-2. Schizophr Res 163, 63–72. [PubMed: 25449710]

MacLean SE, Ward LM, 2014. Temporo-frontal phase synchronization supports hierarchical network for mismatch negativity. Clin Neurophysiol 125, 1604–1617. [PubMed: 24508191]

Martínez A, Hillyard SA, Dias EC, Hagler DJ Jr., Butler PD, Guilfoyle DN, Jalbrzikowski M, Silipo G, Javitt DC, 2008. Magnocellular pathway impairment in schizophrenia: evidence from functional magnetic resonance imaging. J Neurosci 28, 7492–7500. [PubMed: 18650327]

Mathiak K, Rapp A, Kircher TT, Grodd W, Hertrich I, Weiskopf N, Lutzenberger W, Ackermann H, 2002. Mismatch responses to randomized gradient switching noise as reflected by fMRI and whole-head magnetoencephalography. Hum Brain Mapp 16, 190–195. [PubMed: 12112773]

Miyanishi T, Sumiyoshi T, Higuchi Y, Seo T, Suzuki M, 2013. LORETA current source density for duration mismatch negativity and neuropsychological assessment in early schizophrenia. PLoS One 8, e61152. [PubMed: 23577204]

Molholm S, Martinez A, Ritter W, Javitt DC, Foxe JJ, 2005. The neural circuitry of pre-attentive auditory change-detection: an fMRI study of pitch and duration mismatch negativity generators. Cereb Cortex 15, 545–551. [PubMed: 15342438]

Morita K, Miura K, Fujimoto M, Yamamori H, Yasuda Y, Kudo N, Azechi H, Okada N, Koshiyama D, Shiino T, Fukunaga M, Watanabe Y, Ikeda M, Kasai K, Hashimoto R, 2019. Eye-movement characteristics of schizophrenia and their association with cortical thickness. Psychiatry Clin Neurosci 73, 508–509. [PubMed: 31102322]

Mullen TR, Kothe CA, Chi YM, Ojeda A, Kerth T, Makeig S, Jung TP, Cauwenberghs G, 2015. Real-Time Neuroimaging and Cognitive Monitoring Using Wearable Dry EEG. IEEE Trans Biomed Eng 62, 2553–2567. [PubMed: 26415149]

Oknina LB, Wild-Wall N, Oades RD, Juran SA, Ropcke B, Pfueller U, Weisbrod M, Chan E, Chen EY, 2005. Frontal and temporal sources of mismatch negativity in healthy controls, patients at onset of schizophrenia in adolescence and others at 15 years after onset. Schizophr Res 76, 25–41. [PubMed: 15927796]

Oostenveld R, Fries P, Maris E, Schoffelen JM, 2011. FieldTrip: Open source software for advanced analysis of MEG, EEG, and invasive electrophysiological data. Comput Intell Neurosci 2011, 156869. [PubMed: 21253357]

Oostenveld R, Praamstra P, 2001. The five percent electrode system for high-resolution EEG and ERP measurements. Clin Neurophysiol 112, 713–719. [PubMed: 11275545]

Opitz B, Rinne T, Mecklinger A, von Cramon DY, Schroger E, 2002. Differential contribution of frontal and temporal cortices to auditory change detection: fMRI and ERP results. Neuroimage 15, 167–174. [PubMed: 11771985]

Perez VB, Tarasenko M, Miyakoshi M, Pianka ST, Makeig SD, Braff DL, Swerdlow NR, Light GA, 2017. Mismatch Negativity is a Sensitive and Predictive Biomarker of Perceptual Learning During Auditory Cognitive Training in Schizophrenia. Neuropsychopharmacology 42, 2206–2213. [PubMed: 28139679]

Phillips HN, Blenkmann A, Hughes LE, Bekinschtein TA, Rowe JB, 2015. Hierarchical Organization of Frontotemporal Networks for the Prediction of Stimuli across Multiple Dimensions. J Neurosci 35, 9255–9264. [PubMed: 26109651]

Piazza C, Miyakoshi M, Akalin-Acar Z, Cantiani C, Reni G, Bianchi AM, 2016. An Automated Function for Identifying EEG Independent Components Representing Bilateral Source Activity., XIV Mediterranean Conference on Medical and Biological Engineering and Computing 2016. Springer International Publishing, 105–109.

Pion-Tonachini L, Kreutz-Delgado K, Makeig S, 2019. ICLabel: An automated electroencephalographic independent component classifier, dataset, and website. Neuroimage 198, 181–197. [PubMed: 31103785]

Randeniya R, Oestreich LKL, Garrido MI, 2018. Sensory prediction errors in the continuum of psychosis. Schizophr Res 191, 109–122. [PubMed: 28457774]

Rasser PE, Schall U, Todd J, Michie PT, Ward PB, Johnston P, Helmbold K, Case Y, Soyland A, Tooney PA, Thompson PM, 2011. Gray matter deficits, mismatch negativity, and outcomes in schizophrenia. Schizophr Bull 37, 131–140. [PubMed: 19561058]

Rissling AJ, Braff DL, Swerdlow NR, Hellemann G, Rassovsky Y, Sprock J, Pela M, Light GA, 2012. Disentangling early sensory information processing deficits in schizophrenia. Clin Neurophysiol 123, 1942–1949. [PubMed: 22608970]

Rissling AJ, Miyakoshi M, Sugar CA, Braff DL, Makeig S, Light GA, 2014. Cortical substrates and functional correlates of auditory deviance processing deficits in schizophrenia. Neuroimage Clin 6, 424–437. [PubMed: 25379456]

Rissling AJ, Park SH, Young JW, Rissling MB, Sugar CA, Sprock J, Mathias DJ, Pela M, Sharp RF, Braff DL, Light GA, 2013. Demand and modality of directed attention modulate “pre-attentive” sensory processes in schizophrenia patients and nonpsychiatric controls. Schizophr Res 146, 326–335. [PubMed: 23490760]

Rousseeuw P, 1987. Silhouettes: a graphical aid to the interpretation and validation of cluster analysis. J Comput Appl Math 20, 53–65.

Salisbury DF, Polizzotto NR, Nestor PG, Haigh SM, Koehler J, McCarley RW, 2017. Pitch and Duration Mismatch Negativity and Premorbid Intellect in the First Hospitalized Schizophrenia Spectrum. Schizophr Bull 43, 407–416. [PubMed: 27231308]

Schall U, Johnston P, Todd J, Ward PB, Michie PT, 2003. Functional neuroanatomy of auditory mismatch processing: an event-related fMRI study of duration-deviant oddballs. Neuroimage 20, 729–736. [PubMed: 14568447]

Squires NK, Squires KC, Hillyard SA, 1975. Two varieties of long-latency positive waves evoked by unpredictable auditory stimuli in man. Electroencephalogr Clin Neurophysiol 38, 387–401. [PubMed: 46819]

Sterzer P, Adams RA, Fletcher P, Frith C, Lawrie SM, Muckli L, Petrovic P, Uhlhaas P, Voss M, Corlett PR, 2018. The Predictive Coding Account of Psychosis. Biol Psychiatry 84, 634–643. [PubMed: 30007575]

Swerdlow NR, Bhakta S, Chou HH, Talledo JA, Balvaneda B, Light GA, 2016. Memantine Effects On Sensorimotor Gating and Mismatch Negativity in Patients with Chronic Psychosis. Neuropsychopharmacology 41, 419–430. [PubMed: 26062785]

Tada M, Kirihara K, Mizutani S, Uka T, Kunii N, Koshiyama D, Fujioka M, Usui K, Nagai T, Araki T, Kasai K, 2019. Mismatch negativity (MMN) as a tool for translational investigations into early psychosis: A review. Int J Psychophysiol 145, 5–14. [PubMed: 30831138]

Takahashi H, Rissling AJ, Pascual-Marqui R, Kirihara K, Pela M, Sprock J, Braff DL, Light GA, 2013. Neural substrates of normal and impaired preattentive sensory discrimination in large cohorts of nonpsychiatric subjects and schizophrenia patients as indexed by MMN and P3a change detection responses. Neuroimage 66, 594–603. [PubMed: 23085112]

Tateno T, Higuchi Y, Nakajima S, Sasabayashi D, Nakamura M, Ueno M, Mizukami Y, Nishiyama S, Takahashi T, Sumiyoshi T, Suzuki M, 2020. Features of Duration Mismatch Negativity Around the Onset of Overt Psychotic Disorders: A Longitudinal Study. Cereb Cortex.

Thomas ML, Green MF, Hellemann G, Sugar CA, Tarasenko M, Calkins ME, Greenwood TA, Gur RE, Gur RC, Lazzeroni LC, Nuechterlein KH, Radant AD, Seidman LJ, Shiluk AL, Siever LJ, Silverman JM, Sprock J, Stone WS, Swerdlow NR, Tsuang DW, Tsuang MT, Turetsky BI, Braff DL, Light GA, 2017. Modeling Deficits From Early Auditory Information Processing to Psychosocial Functioning in Schizophrenia. JAMA Psychiatry 74, 37–46. [PubMed: 27926742]

Umbricht D, Krljes S, 2005. Mismatch negativity in schizophrenia: a meta-analysis. Schizophr Res 76, 1–23. [PubMed: 15927795]

Wynn JK, Sugar C, Horan WP, Kern R, Green MF, 2010. Mismatch negativity, social cognition, and functioning in schizophrenia patients. Biol Psychiatry 67, 940–947. [PubMed: 20074704]

Yamasue H, Yamada H, Yumoto M, Kamio S, Kudo N, Uetsuki M, Abe O, Fukuda R, Aoki S, Ohtomo K, Iwanami A, Kato N, Kasai K, 2004. Abnormal association between reduced magnetic mismatch field to speech sounds and smaller left planum temporale volume in schizophrenia. Neuroimage 22, 720–727. [PubMed: 15193600]

Youn T, Park HJ, Kim JJ, Kim MS, Kwon JS, 2003. Altered hemispheric asymmetry and positive symptoms in schizophrenia: equivalent current dipole of auditory mismatch negativity. Schizophr Res 59, 253–260. [PubMed: 12414082]

Highlights

- Mismatch negativity and P3a are reduced in schizophrenia at a scalp electrode of Fz.
- It is unclear how cortical sources contribute to MMN and P3a responses at Fz.
- Contributions of 11 cortical source components were back projected to Fz.
- Schizophrenia patients and controls showed comparable source contributions to Fz.
- Patients showed reduced source-level responses quantified from frontal sources.

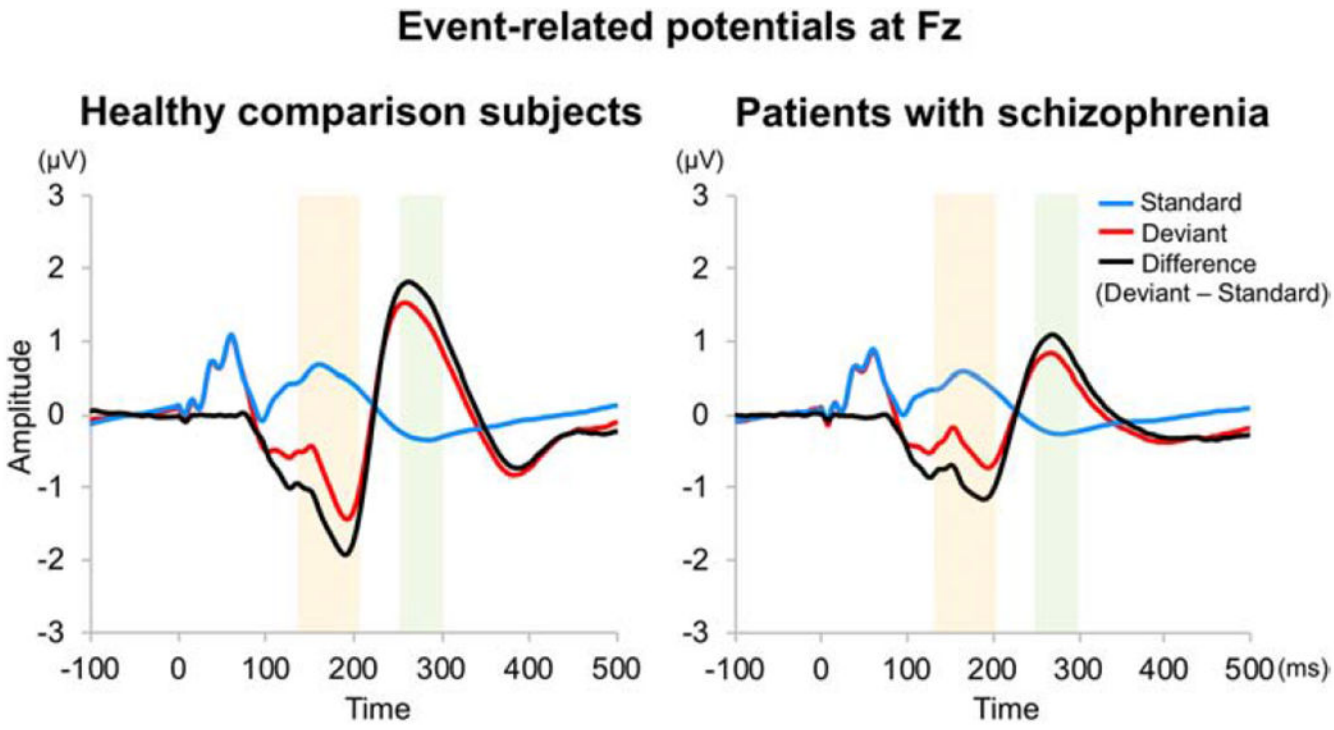

Figure 1.

Event-related potentials at scalp Fz.

Legend: Orange color shadow indicates the time window of mismatch negativity (135–205 ms), and green color indicates that of P3a (250–300 ms). Mismatch negativity and P3a amplitude reflect back-projected surface potential estimates at Fz using an average reference.

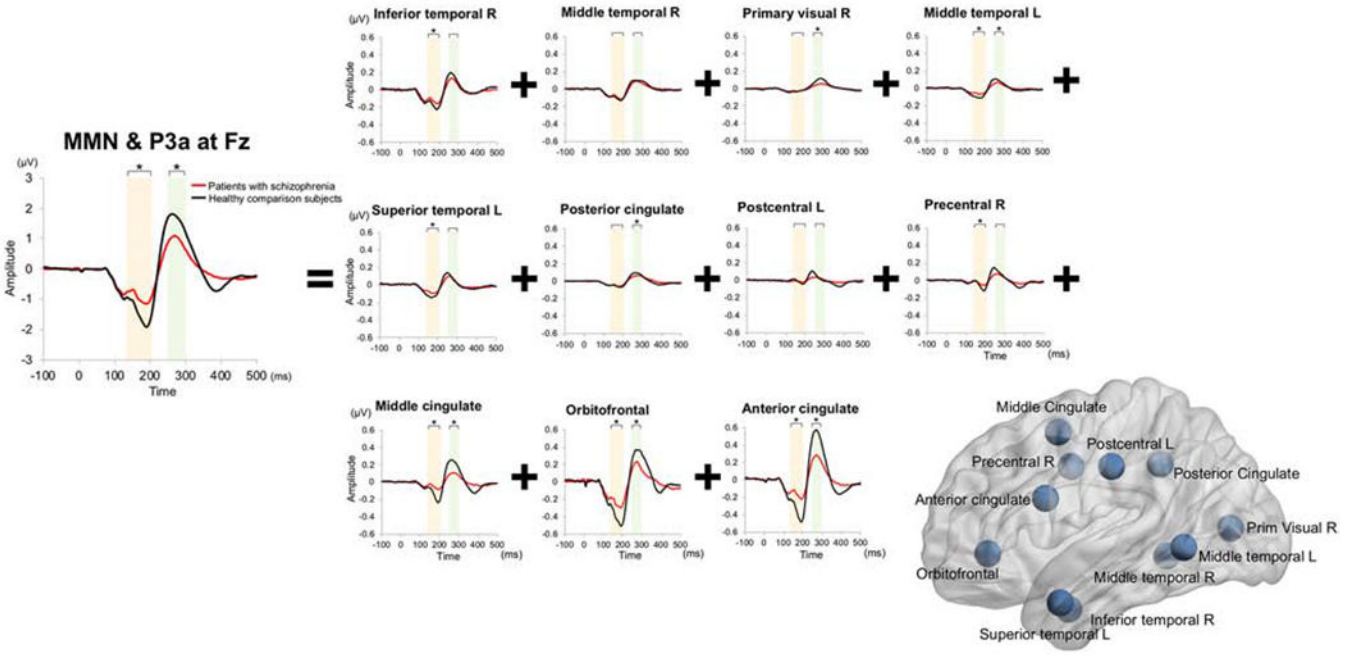

Figure 2.

Source components whose sum is equivalent to mismatch negativity and P3a at scalp Fz in each group

Legend: Orange color shadow indicates the time window of mismatch negativity (135–205 ms), and green color indicates that of P3a (250–300 ms). Asterisks indicate statistical significance of $p < 0.05$ adjusted to false discovery rate with 2 responses for MMN and P3a amplitude (μV) at Fz, and $p < 0.05$ adjusted to false discovery rate with 2 responses × 11 source locations for MMN and P3a amplitude (μV) at source locations. Mismatch negativity and P3a amplitude reflect back-projected surface potential estimates at Fz using an average reference.

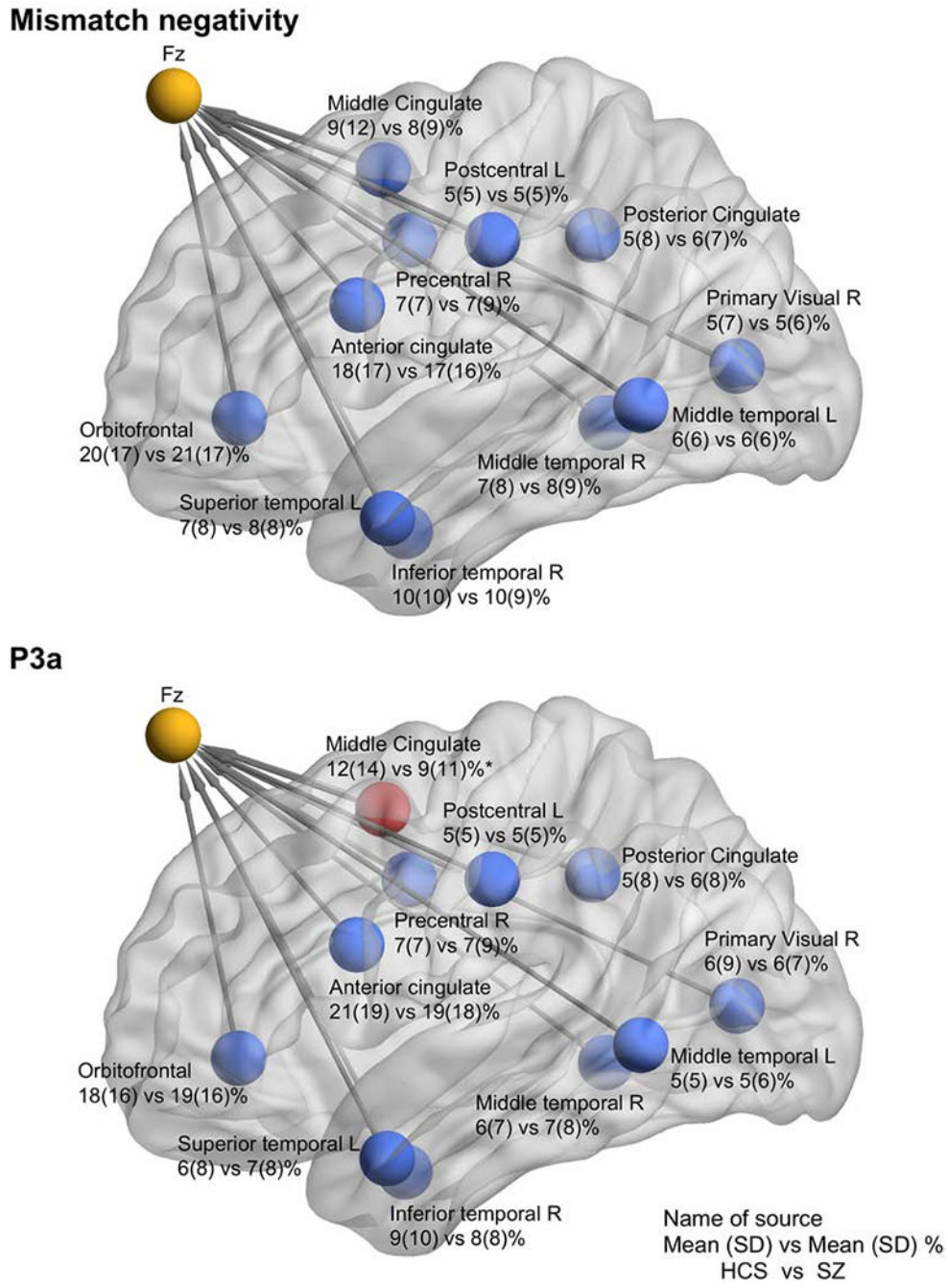

Figure 3.

Contribution rates (%) of source components to mismatch negativity (MMN) and P3a at scalp Fz

Legend: The asterisk and red sphere indicate statistical significance of $p < 0.05$ adjusted to false discovery rate with 2 responses × 11 source locations.

Abbreviations: HCS, healthy comparison subjects; L, left; R, right; SD, standard deviation; SZ, schizophrenia.

Int J Psychophysiol. Author manuscript; available in PMC 2022 March 01.

Table 1

Difference of event-related potentials (μV) in each region between healthy comparison subjects and schizophrenia patients

	Healthy comparison subjects		Schizophrenia patients		*d*	*df*	*t*	*p*
	Mean	**SD**	**Mean**	**SD**				
Mismatch negativity								
Fz	−1.47	1.06	−0.94	0.81	−0.55	1036	−9.00	**1.1×10^{-18}***
Inferior temporal R	−0.17	0.23	−0.13	0.22	−0.21	427.0	−2.41	**0.016***
Middle temporal R	−0.10	0.14	−0.09	0.14	−0.08	884.1	−1.26	0.208
Primary visual R	−0.03	0.09	−0.03	0.07	−0.05	959.3	−0.73	0.468
Middle temporal L	−0.09	0.14	−0.06	0.11	−0.30	736.4	−4.33	**1.7×10^{-5}***
Superior temporal L	−0.12	0.17	−0.08	0.15	−0.26	563.9	−3.44	**0.001***
Posterior cingulate	−0.06	0.12	−0.05	0.12	−0.07	1246.0	−1.38	0.169
Postcentral L	−0.01	0.16	−0.01	0.11	−0.03	940.2	−0.44	0.659
Precentral R	−0.06	0.21	−0.03	0.13	−0.15	904.1	−2.51	**0.012***
Middle cingulate	−0.14	0.33	−0.05	0.15	−0.35	552.1	−5.09	**4.8×10^{-7}***
Orbitofrontal	−0.41	0.52	−0.24	0.39	−0.36	909.9	−5.99	**3.0×10^{-9}***
Anterior cingulate	−0.36	0.45	−0.17	0.27	−0.52	546.7	−7.17	**2.5×10^{-12}***
P3a								
Fz	1.62	1.28	0.93	0.93	0.61	1036	9.97	**2.0×10^{-22}***
Inferior temporal R	0.15	0.30	0.10	0.20	0.19	319.6	2.07	0.039
Middle temporal R	0.10	0.15	0.08	0.14	0.11	863.2	1.59	0.111
Primary visual R	0.10	0.13	0.05	0.09	0.46	881.6	7.33	**5.4×10^{-13}***
Middle temporal L	0.08	0.14	0.05	0.10	0.24	685.5	3.52	**4.6×10^{-4}***
Superior temporal L	0.07	0.18	0.07	0.15	0.01	555.6	0.19	0.852
Posterior cingulate	0.09	0.17	0.06	0.14	0.16	1084.3	2.98	**0.003***
Postcentral L	0.03	0.15	0.03	0.13	0.0003	1069.1	0.004	0.996
Precentral R	0.08	0.24	0.06	0.17	0.12	961.9	2.14	0.033
Middle cingulate	0.23	0.51	0.10	0.30	0.31	633.0	4.56	**6.1×10^{-6}***
Orbitofrontal	0.35	0.77	0.19	0.49	0.24	811.4	3.94	**8.8×10^{-5}***
Anterior cingulate	0.52	0.69	0.25	0.42	0.47	554.4	6.48	**2.1×10^{-10}***

Legend: *d* indicates effect size of Cohen's *d*. Asterisks and bold indicate statistical significance of $p < 0.05$ adjusted to false discovery rate with 2 responses for MMN and P3a at Fz, and $p < 0.05$ adjusted to false discovery rate with 2 responses × 11 source locations for MMN and P3a at source locations.

Abbreviation: L, left; R, right; SD, standard deviation.

Table 2

Difference of contribution rate (%) of event-related potentials in each region to those at Fz between healthy comparison subjects and schizophrenia patients

	Healthy comparison subjects		Schizophrenia patients		*df*	*t*	*p*
	Mean	**SD**	**Mean**	**SD**			
MMN							
Inferior temporal R	10.3	10.1	9.7	9.0	393.4	1.07	0.273
Middle temporal R	7.0	8.0	8.2	8.5	887.6	−1.76	0.072
Primary visual R	4.7	7.2	5.0	5.6	939.5	−0.41	0.683
Middle temporal L	5.7	6.0	5.7	5.8	828.2	0.44	0.650
Superior temporal L	7.2	8.0	7.7	7.8	598.9	−0.57	0.588
Posterior cingulate	4.9	7.6	5.8	7.2	1214.5	−1.90	0.062
Postcentral L	5.3	4.8	5.4	5.2	1197.4	0.08	0.934
Precentral R	6.9	7.2	7.3	8.5	1260.0	−0.44	0.660
Middle cingulate	9.3	11.9	7.7	8.9	725.7	2.67	0.005
Orbitofrontal	20.3	16.5	20.8	17.2	1112.4	0.003	0.984
Anterior cingulate	18.3	16.9	16.8	16.4	754.6	1.72	0.085
P3a							
Inferior temporal R	8.9	9.6	8.2	8.0	369.7	1.10	0.264
Middle temporal R	6.0	7.1	7.2	7.7	895.3	−2.09	0.042
Primary visual R	6.2	8.6	5.6	7.0	959.8	1.49	0.135
Middle temporal L	4.6	4.7	5.2	6.0	887.9	−1.61	0.114
Superior temporal L	6.3	7.9	7.2	7.8	609.5	−1.47	0.161
Posterior cingulate	5.4	7.9	6.1	7.9	1253.6	−1.35	0.187
Postcentral L	4.9	4.8	5.4	5.4	1217.3	−1.32	0.191
Precentral R	6.6	7.3	7.2	8.8	1263.2	−1.07	0.293
Middle cingulate	11.9	14.0	9.3	10.6	733.4	3.42	**5.0×10^{-4}***
Orbitofrontal	18.3	16.3	19.4	16.1	1082.1	−0.77	0.446
Anterior cingulate	21.0	18.5	19.2	17.7	749.2	1.76	0.077

Legend: Asterisks and bold indicate statistical significance of $p < 0.05$ adjusted to false discovery rate with 2 responses × 11 source locations.

Abbreviation: L, left; R, right; SD, standard deviation.